Proceedings of ASME Turbo Expo 2012
GT2012
June 11-15, 2012, Copenhagen, Denmark

GT2012-69636

UNSTEADY AERODYNAMICS OF A CENTRIFUGAL COMPRESSOR STAGE – VALIDATION OF TWO DIFFERENT CFD SOLVERS

Oliver Borm*
Institute for Thermal Turbomachinery and Machine Dynamics
Graz University of Technology
Inffeldgasse 25A
A-8010 Graz, Österreich
oli.borm@web.de

Hans-Peter Kau
Institute for Flight Propulsion
Technische Universität München
Boltzmannstr. 15
D-85748 Garching b. München, Deutschland

ABSTRACT

The unsteady flow field of a centrifugal compressor stage with vaned diffuser has been numerically investigated. Three dimensional steady as well as unsteady numerical simulations have been carried out with the CFD programs Numeca and OpenFOAM. The investigated numerical approaches range from a steady state mixing-plane simulation to an unsteady full annulus 360° computation. The numerical investigation was done at 80% design speed with the Spalart-Allmaras as well as the k-ω SST turbulence model. All numerical simulations were compared to the experiments in the compressor map. The velocity field of one operating point near the surge line was analysed in more detail. Similarities and differences between numerical and experimental results are discussed and their causes and effects pointed out.

NOMENCLATURE

$\vec{c}$	Absolute velocity
$\vec{w}$	Relative velocity
$\vec{u}$	Circumferential velocity
$\vec{\omega}$	Angular velocity
p	Pressure
T	Temperature
c_p	Specific heat capacity at constant pressure
$\varkappa$	Ratio of specific heat capacities
μ_t	Turbulent viscosity
$\dot{m}_{Norm}$	Massflow normalised to standard conditions
Π_{tt}	$= p_{t,E}/p_{t,I}$ Total pressure ratio
η_s	$= \frac{\Pi_{tt}^{1-1/\varkappa}-1}{T_{t,E}/T_{t,I}-1}$ Isentropic efficiency
Φ	Arbitrary field
$\vec{r}$	Position vector
φ	Circumferential direction
$()_{,I}$	Impeller
$()_{,D}$	Diffuser
$()'$	Values referring to the relative coordinate system

INTRODUCTION

Modern highly loaded centrifugal compressors with vaned diffusers allow obtaining large total pressure ratios with a small compressor size. Due to the compact size the radial distance between impeller trailing edge and diffuser leading edge will be short. As known at least since Eckardt [2] the outflow of centrifugal compressors is highly inhomogeneous in axial and azimuthal direction. In conjunction with the small radius ratio the inflow to the vaned diffuser will be therefore very unsteady. The numerically investigated centrifugal compressor consists of an unshrouded impeller (Fig. 1) and a wedge-type diffuser. An extensive measurement series of this centrifugal compressor was carried out by Ziegler [3]. Measurement probes were applied

*This work has been conducted at the Institute for Flight Propulsion of the Technische Universität München as part of the dissertation of the first author [1].

to determine pressure and temperature of the fluid. Furthermore, the Laser-2-Focus (L2F) method was used by Ziegler [3] to measure the two dimensional fluid velocity vector at different meridional positions of the machine at one operating point near the surge line of the 80% speed line. For a complete overview of the measurement data sets the reader may refer to Ziegler [3]. The stage geometry as well as the detailed steady and unsteady measurement data were published as an open CFD test case. Therefore, the experimental results are well suited to validate numerical simulations of centrifugal compressors.

Within this work three dimensional steady and unsteady simulations have been carried out with two different density-based CFD solvers. Due to the rotation of the impeller, the limited computational resources and in general the different blade number of the blade rows, the modelling of the interface between rotor and stator is very challenging. The following numerical approaches for turbomachinery have been evaluated:

- mixing-plane approach
- domain-scaling approach
- non-linear harmonic method
- full annulus 360° simulation

Previous studies have already been done by Boncinelli et al. [4] and Smirnov et al. [5] with different CFD codes in order to investigate the rotor stator interaction. They did steady and unsteady simulations of this test case. Thus, they are a good basis for comparison of the numerical results. Furthermore the centrifugal impeller was experimentally investigated with a vaneless diffuser. For this configuration Borm et al. [6] already analysed the behaviour of the CFD codes Numeca and OpenFOAM.

NUMERICAL MODEL

The numerical model is almost identical to the steady state simulations with a vaneless diffuser [6] where the numerical setup is described in detail.

Solver Description

Both investigated solvers are formally second order accurate in space and time. The space discretisation is different between the solvers, whereas the time integration is done in both cases with a dual-time stepping method.

Numeca The FINE/Turbo solver from Numeca is based on block-structured meshes. The convective fluxes are evaluated with the Jameson-Schmidt-Turkel scheme. Therefore the conservation equations for rotating turbomachinery are formulated with the relative velocity.

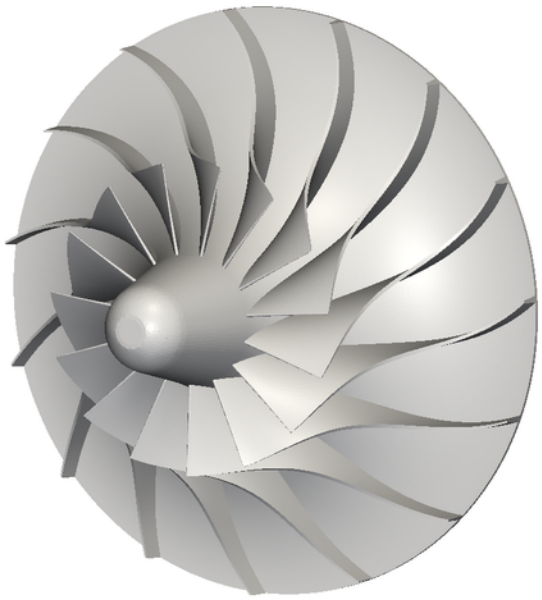

FIGURE 1. IMPELLER

OpenFOAM The free CFD software OpenFOAM is based on arbitrary polyhedral meshes. A new solver called *transonicUnsteadyMRFDyMFoam* which is based on an approximate Riemann solver (HLLC) was developed by Borm et al. [7] within OpenFOAM. Nevertheless, for convenience reasons, the presented simulations and results are in the following only referred to as OpenFOAM. Thereby, the space discretisation is of second order accuracy, the primitive variables are linearly reconstructed from the cell centre to the face centre. This Taylor series reads for an arbitrary scalar field Φ as follows:

$$\Phi(\xi) = \Phi(\xi_0) + (\xi - \xi_0) \bullet \frac{\mathrm{d}\Phi(\xi_0)}{\mathrm{d}\xi} \tag{1}$$

For a vector field Eqn. (1) has to be processed for each component separately. It is important to note that the occurring scalar product of the distance vector by the tensor is not commutative. Thus the Taylor series for an arbitrary vector field $\vec{\Phi}$ has to be written as:

$$\vec{\Phi}\left(\vec{\xi}\right) = \vec{\Phi}\left(\vec{\xi_0}\right) + \left(\vec{\xi} - \vec{\xi_0}\right) \bullet \nabla\vec{\Phi}\left(\vec{\xi_0}\right) \tag{2}$$

Turbomachinery is characterised by rotating blade rows. Due to this rotation the Cartesian components of the unit vectors of the relative coordinate system of the rotor is

changing in time. In the case of steady state simulations the Navier-Stokes-Equations are solved in the relative reference frame and thus there is normally no need to move the mesh. In order to account for the impeller rotation an additional source term is present in vector conservation equations, like the momentum equation, because of the temporal change of the direction of the unit vectors. This leads to the following relationship for the time variation of an arbitrary vector $\vec{\Phi}$ between the absolute and the relative coordinate system with the additional source term:

$$\frac{\mathrm{d}}{\mathrm{d}t}\int_{V(t)} \vec{\Phi}\ \mathrm{d}V = \frac{\mathrm{d}'}{\mathrm{d}t}\int_{V(t)} \vec{\Phi}\ \mathrm{d}V + \int_{V(t)} \left(\vec{\omega}\times\vec{\Phi}\right)\ \mathrm{d}V \quad (3)$$

For unsteady simulations the impeller mesh is rotating about the rotation axis. In order to account for this effect the conservation equations are based on an Arbitrary Lagrangian Eulerian (ALE) formulation, as described for example by Hirt et al. [8]. The boundary velocity of the control volumes is then equal to the circumferential velocity $\vec{u} = \vec{\omega}\times\vec{r}$. In contrast to the steady state simulations, where no mesh motion is present, no special source terms apply in the momentum equation in the unsteady case. The disadvantage of this time integration is, that the effect of the source term from Eqn. (3) is a result of the computation and cannot be prescribed a priori for each time step. For a faster convergence in the inner iterations of the dual-time stepping it is favourable to prescribe this source term a priori. Therefore, an alternative ALE formulation was chosen for rotating meshes in unsteady simulations. It is assumed that the mesh motion is restricted to a rigid body rotation about the z-axis. The radial velocity c_r and circumferential component of the absolute velocity c_u is computed after each time step from the Cartesian components of the absolute velocity and the position vector of each cell centre, as the directions of the unit vectors of a cylindrical coordinate system is not changing due to rotation. After the mesh motion is applied in the next time step, the Cartesian velocity components are computed based on the radial c_r and circumferential component of the absolute velocity c_u and the new position vector of each cell centre. Thus, the time integration of the momentum equation can be interpreted as it would be done in the relative frame of reference. This procedure is also applied to all values from old time steps which are needed for the used three-point backward time integration. Therefore, the source term from Eqn. (3) has to be applied a priori in the time integration within the relative coordinate system.

TABLE 1. INLET BOUNDARY CONDITIONS

Parameter	$p_{t,abs}$ [Pa]	$T_{t,abs}$ [K]	$\frac{\vec{c}}{\lvert\vec{c}\rvert}$ [-]	μ_t $[\frac{m^2}{s}]$
Value	101300	288.15	$\begin{pmatrix}0\\0\\1\end{pmatrix}$	0.0001

Boundary Conditions

The simulations were performed on operating points at 80% design speed. Air was used as fluid and considered as perfect gas with $c_p = 1004.5\ J/(kg\ K)$ and $\varkappa = 1.4$. The laminar viscosity was modelled temperature dependent by the law of Sutherland. Contrary to the experiments, the calculations were conducted at standard inlet conditions. This approach has the advantage that all CFD results are already normalised. In this way they can be directly analysed without further conversion, which is convenient for larger mesh sizes. The inlet boundary conditions for all computations are shown in Tab. 1. Solid walls are of no-slip type and adiabatic.

A constant static pressure was specified at the outlet, so that the normalised massflow adjusts according to the experiments, with an error of $\pm 1\%$, which is identical to the experimental uncertainty. All other primitive variables are evaluated at the outlet with the zero gradient boundary condition. In OpenFOAM a new outlet boundary condition was implemented. Hence, the velocity is evaluated with the zero gradient boundary condition in each face of the outlet patch. If the velocity component normal to each face becomes negative, this component is set to zero. Furthermore, for those faces where the normal velocity component is less or equal than zero, a zero static pressure gradient boundary condition is specified.

Measurement Positions

This paper focuses on the measurement positions 2M', 4M and 7M as shown in Fig. 2. Labeling of the positions was done according to the experimental investigations [3]. The 2M' conical measurement surface is located shortly before the end of the impeller channel and is enclosed on each side by the rotor blades. The 4M cylindrical surface is positioned upstream of the vaned diffuser, whereas the cylindrical surface 7M is shortly downstream of the vaned diffuser.

Overview CFD Models

An overview of the investigated CFD models is given in Tab. 2. The table lists the combination of CFD solver, turbulence model, either Spalart-Allmaras (SA) or k-ω SST (SST) model, numerical approach and the number of blades in each blade row of the model. Normally only one param-

TABLE 2. CFD MODELS

№	CFD Solver	Turbulence Model	Numerical Approach	№ Impeller Blades	№ Diffuser Vanes	№ Meshed Impeller Passages	№ Meshed Diffuser Passages	Cells Impeller	Cells Diffuser
1	Numeca	SA	Steady	15	23	1	1	804 k	621 k
2	Numeca	SST	Steady	15	23	1	1	804 k	621 k
3	Numeca	SA	DS Unsteady	15	30	1	2	3.51 M	1.46 M
4	Numeca	SST	DS Unsteady	15	30	1	2	3.51 M	1.46 M
5	OpenFOAM	SST	DS Unsteady	15	30	1	2	1.22 M	993 k
6	Numeca	SA	DS NLH12	15	30	1	2	3.51 M	1.46 M
7	Numeca	SA	DS NLH13	15	30	1	2	3.51 M	1.46 M
8	Numeca	SA	NLH12	15	23	1	1	804 k	621 k
9	Numeca	SA	NLH13	15	23	1	1	804 k	621 k
10	Numeca	SA	360° Unsteady	15	23	15	23	12.06 M	14.28 M

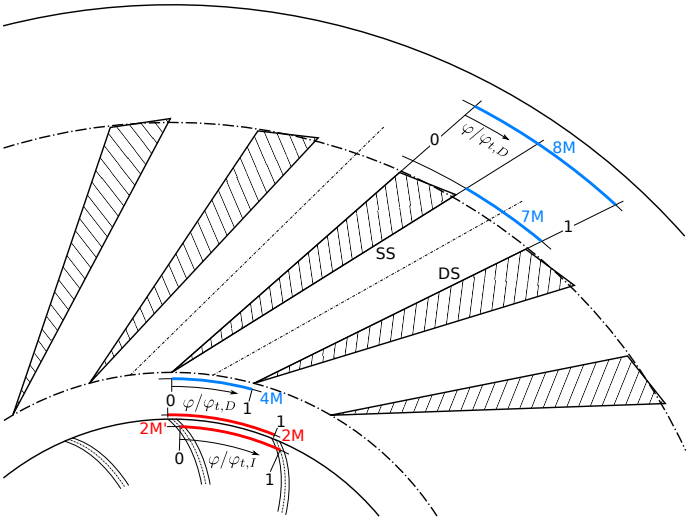

FIGURE 2. MEASUREMENT POSITIONS

eter is different between each model in order to be able to assign the changes between the simulations to this parameter. Both steady state models (№ 1-2) are using the *mixing-plane* approach. The *domain-scaling* (DS) approach with equal pitches of the rotor and stator domain was also employed (№ 3-7). Therefore, the number of diffuser vanes was increased in order to apply periodic boundary conditions. Hence, to keep the same overall geometric blockage in the diffuser row, the thickness of the wedge-type diffuser vanes was scaled. Whereas the real number of blades in each blade row was used in a full annulus 360° simulation (№ 10).

Furthermore, simulations with the *Non-Linear Harmonic* method (NLH) were carried out in the frequency domain (№ 6-9). The NLH method is able to simulate multistage turbomachinery with unequal pitches in each blade row, while using only one passage per blade row. Thus, for each perturbation in the particular blade row, transport equations for a discrete number of harmonics are solved. In order to obtain an unsteady time signal for the three-dimensional flow field based on the frequency domain an inverse fast Fourier transformation is carried out. The two digits of the NLH computation names represents the number of perturbations, in this case the perturbations are always one, and the number of calculated harmonics, either two or three. All computations in the frequency domain are using exclusively the Spalart-Allmaras turbulence model.

Additionally the mesh sizes of the different models as well as the number of meshed passages is given in Tab. 2. The meshes for the Numeca simulations were created with AutoGrid from Numeca. For the full annulus 360° computation (№ 10) each passage of the mesh from computation № 9 was repeated in circumferential direction with the corresponding number of blades in each blade row. Thus the resolution of one blade passage is relatively coarse, so that the complete full annulus 360° mesh does not exceed 30 M cells.

The OpenFOAM impeller mesh was also generated with Numeca AutoGrid and is identical to the numerical investigation with vaneless diffuser [6]. Whereas the surface mesh of the scaled diffuser for the OpenFOAM simulation was created with gmsh [9]. Based on this surface mesh, prism

layers were generated at solid walls and the remaining volume was meshed with tetrahedral cells in enGrid [10], because gmsh does not have these capabilities. On the other hand the surface meshing is much faster in gmsh rather than in enGrid. The wall distance in the first cell has to be very small if Low-Reynolds number turbulence models are used. Prism cells retain in contrast to tetrahedral cells good mesh qualities even with small wall distances. The OpenFOAM diffuser mesh consists of 553 k tetrahedral and 442 k prism cells.

RESULTS

Global Results

The centrifugal compressor with vaned diffuser was investigated at 80% design speed within steady as well as unsteady simulations, as there are neither L2F nor probe measurements available at 100% design speed. Thus, there is no additional benefit from numerically investigating the 100% speed line even if it would be very interesting due to the transonic flow behaviour. The compressor map with experimental and numerical results is shown in Fig. 3. The naming of the operating points was taken from the experimental investigations by Ziegler [3]. Unsteady L2F measurements were only conducted at operating point P1. Thus and due to the large numerical effort, the unsteady calculations with Numeca were limited to operating point P1.

The massflow of the numerical results was evaluated in measurement position 8M as shown in Fig. 2. Contrary to that, in the experimental investigation the massflow was measured in an exhaust box after a relatively long straight section. If leakage flows can be neglected the time averaged massflow should be identical in all sections. The averaging of primitive variables from experimental and numerical results in position 8M was done consistently as described in detail by Ziegler [3]. Based on these averaged variables the total pressure ratio as well as the isentropic efficiency were computed from each inlet (I) to position 8M (E). The inlet duct which is present in the experimental investigation was neglected in the numerical model. Thus, the losses in the inlet duct are not acquired in the balances of the numerical results. Due to the low back pressure in operating point S1, a shock occurs in the throat of the diffuser. Unfortunately even in the steady state calculations with mixing-plane the position of the shock is moving periodically. The operating points S1 which are shown in Fig. 3 are thus an arithmetic average over one period. Hence there is no steady state choking flow measurable at position 8M.

The unsteady as well as the time averaged results of the global data from the Numeca simulations in operating point P1 were plotted. However, the time evolutions of the unsteady OpenFOAM results are not shown and thus only

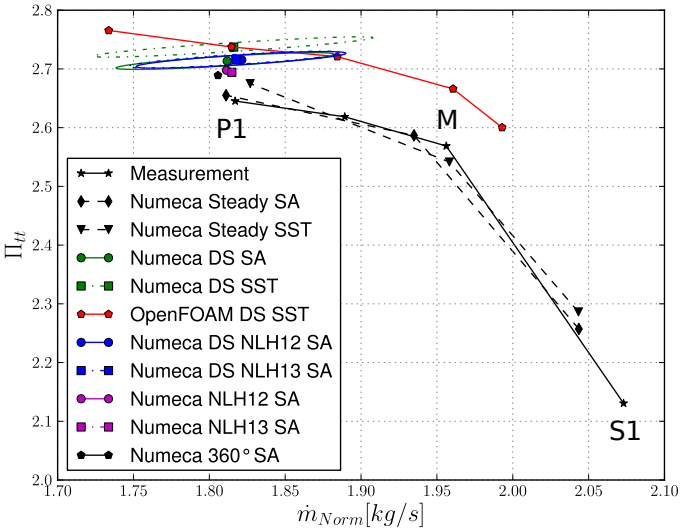

FIGURE 3. COMPRESSOR MAP

the time averaged global results are presented. The steady speed lines of the numerical results show a very good agreement with the experimental data in Fig. 3. At operating point P1 the total pressure ratio has a maximum difference of 0.37%. This should not exceed the measurement uncertainty. Contrary to that, the time averaged speed line of the unsteady OpenFOAM results show an almost constant larger total pressure ratio compared to the experimental speed line, whereas the slope of this speed line has good agreement with the experimental data. Furthermore, all time averaged unsteady Numeca results show a larger total pressure ratio at operating point P1 compared to the measurements. The time averaged unsteady Numeca and OpenFOAM result with k-ω SST turbulence model are nearly identical. The minimum total pressure ratio difference between experimental and NLH13 computation with real diffuser blade count is 1.85%, whereas the unsteady Numeca computation with k-ω SST turbulence model and scaled diffuser vane has a difference of 3.47%. All computations with scaled diffuser vane are showing a larger total pressure ratio compared to the results with real diffuser blade count. Also the results with the k-ω SST turbulence model have a larger total pressure ratio compared to the Spalart-Allmaras model. These results are in good agreement with the investigations from Smirnov et al. [5] and Hoffmann et al. [11]. The differences in the global results between the simulations in the time and frequency domain are almost negligible. The full annulus 360° simulation shows a slightly smaller massflow with almost identical global results compared to the corresponding NLH simulations. When quantifying the difference between experimental and numerical results some uncertainties, i.a. Reynolds number, adiabatic walls, tip

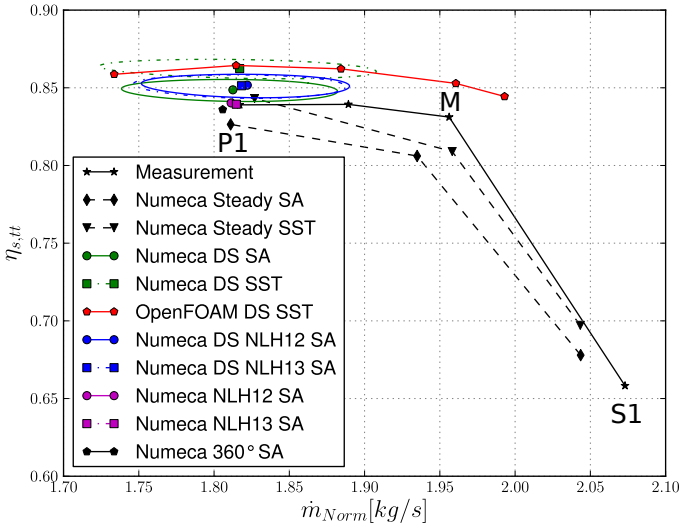

FIGURE 4. ISENTROPIC TOTAL-TOTAL EFFICIENCY

gap size, fillet radius and hot geometry, have to be taken into account. The influence of these uncertainties on the compressor map was already discussed by Borm et al. [6] for the results with vaneless diffuser but can also applied to the simulations with vaned diffuser. One should consider that it is more important for CFD results to capture the trend precisely rather than to predict absolute values, as already explained in detail by Denton [12].

The isentropic efficiency map which is based on total variables is shown Fig. 4. The result of the steady computation with k-ω SST turbulence model has an increased efficiency compared to the simulation with Spalart-Allmaras model. Furthermore, both steady state results are showing a good agreement with the experimental data. The time averaged results of the unsteady simulations have a similar behaviour of the isentropic efficiency compared to the total pressure ratio. The NLH computations with real diffuser blade count have an almost perfect accordance with a maximum difference of 0.041% compared to the measured efficiency. On the other hand the time averaged OpenFOAM simulation with k-ω SST turbulence model has a larger efficiency of about 2.54%. However, the slope of the efficiency of the OpenFOAM computation between the operating points M and P1 is in a better agreement to the experimental results than the steady state Numeca computations.

Measurement Position 7M

The outflow of the vaned diffuser is investigated in more detail. Only time averaged experimental results from Ziegler [3] are available at this measurement position. Thus, the primitive variables from the unsteady numerical results were time averaged for a comparison with the measurements. Based on these time averaged primitive variables the total pressure and Mach number is computed. In contrast to that these values were measured directly with the probe. The total pressure is shown in Fig. 5 at measurement position 7M for one diffuser blade passage. For the one passage models with the real diffuser blade count, only one diffuser passage was simulated. However, for domain-scaling and the full annulus 360° computations only one of the diffuser vane passages was taken into account.

The experimental result show an area with higher total pressure at nearly 50% span height between mid channel and pressure side. As known from the experimental results from Ziegler, the azimuthal position of the maximum total pressure value at this radial gap size of 1.04 is nearly independent from the operating point. The total pressure level of the steady computations is comparable to the experimental results. However, the area with higher total pressure of the steady simulations indeed lies in the corner suction side/casing in contrast to the experimental result. This trend was also observed by Hoffmann et al. [11]. The steady state results with k-ω SST turbulence model show also an extension of higher total pressure in the area near the pressure side. But it has to be noted, that the highest values of total pressure are near the suction side and casing.

In all time averaged results of the unsteady simulations the total pressure level is higher than in the experimental results. This could already be guessed from the compressor map in Fig. 3. So that the results are Mach number similar, the normalised massflows of the numerical simulations have to be identical to the experimental results. Therefore the static pressure at the numerical outlet has to be higher than in the measurements. This can be attributed to the effect, that lower losses are predicted in the vaned diffuser. The area with the larger total pressure values is shifted to the pressure side compared to the steady state results. All results with Spalart-Allmaras turbulence model and the real diffuser blade count are almost identical. The same is true for the simulations with Spalart-Allmaras model and the scaled diffuser. Nevertheless, the characteristic area of higher total pressure is different between these two diffuser configurations. Both results with scaled diffuser and k-ω SST turbulence model show a larger area of higher total pressure. Compared to the results with the Spalart-Allmaras model this area is shifted in both results towards the pressure side. The result of the OpenFOAM simulation shows a slightly better characteristic of the total pressure distribution than the result of the Numeca computation. A similar difference between steady and time averaged unsteady results was also observed by Grates [13].

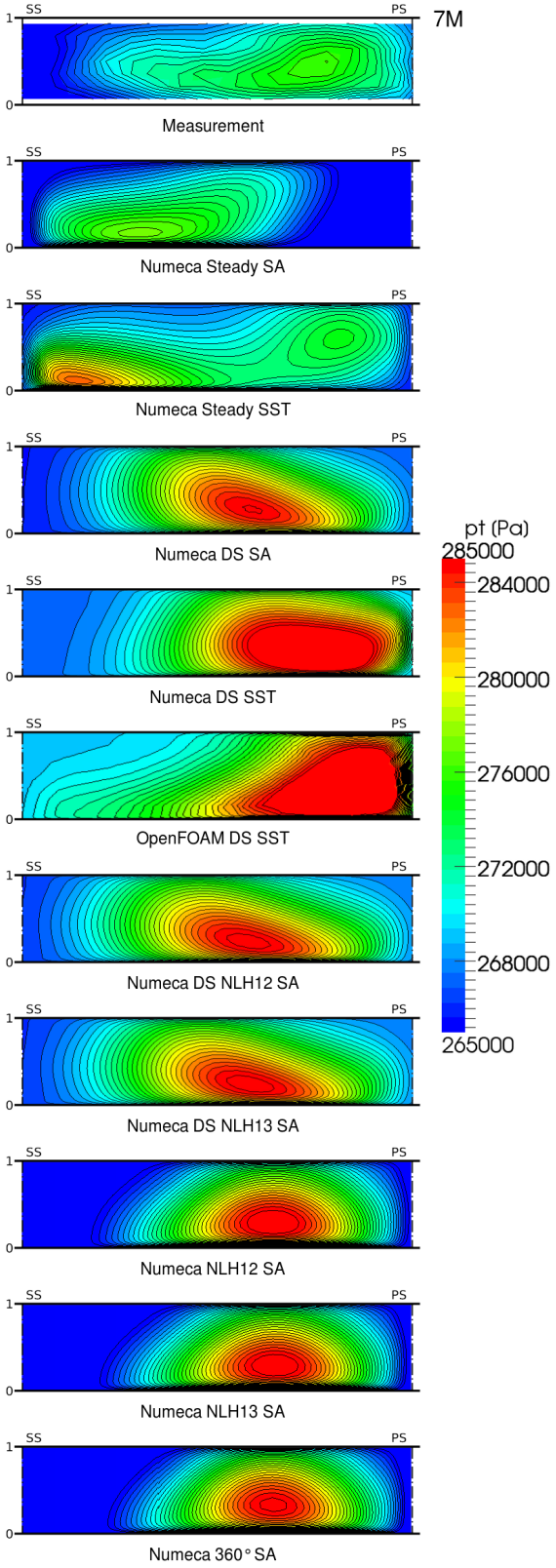

FIGURE 5. TOTAL PRESSURE - POSITION 7M

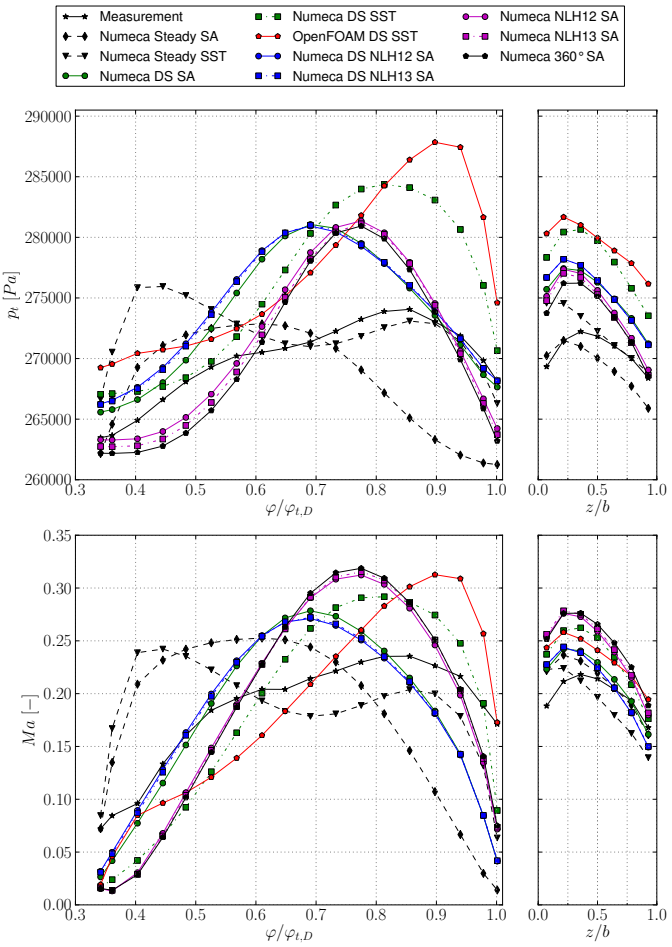

FIGURE 6. AVERAGED VALUES - POSITION 7M

The aforementioned time averaged total pressure and Mach number was evaluated at the experimental probe points. All experimental and numerical results were radial velocity flux weighted averaged in axial and azimuthal direction according to Ziegler [3]. The averaged results are plotted in normalised circumferential ($\varphi/\varphi_{t,D}$) and span height (z/b) in Fig. 6. The unsteady results overestimate the maximum level of both variables. In contrary to the averaged steady results, the azimuthal position of the peak values are better predicted. Additionally, the results with the k-ω SST turbulence model have again the best agreement with the measurements. The time averaged unsteady OpenFOAM result reproduces the axial averaged characteristic of total pressure and Mach number best. In particular, only this numerical result predicts the turning point of the experimental characteristic at about 40% diffuser pitch. The results from Boncinelli et al. [4] also show an offset to the suction side of the peak values for this centrifugal compressor. Although

all unsteady results have a positive offset of the circumferential averaged variables in Fig. 6, the characteristic can be captured well. Compared to the steady results, the slopes of the averaged unsteady results have a better agreement to the experimental data.

Measurement Position 2M'

The unsteady outflow of the impeller is analysed in measurement position 2M' (cf. Fig. 2). The numerical results and the experimental L2F measurements from Ziegler [3] of the relative velocity magnitude are shown in Fig. 7. The unsteady results are presented relative to the impeller rotation. For an improved visualisation the single frames are combined to an animation*. The blade border and the radial projection of the diffuser leading edge are plotted with black lines. Unfortunately, the optical measurements were only done in the middle area of the channel due to laser reflections at the walls. Thus, the measurement window is also plotted. The discrete L2F probe positions are visualised in the top picture of the figure. Due to restrictions of the measurement system the L2F probe points and the measurement window are different for each timestep. For a detailed description of the measurement system and the experimental setup the reader may refer to Bramesfeld [14]. As also explained by Bramesfeld the experimental time resolution with 15 rotor-stator positions for one rotor passage is relatively coarse. Thus, the experimentally determined rotor-stator positions are afflicted with a large bandwidth. Furthermore, the experimental determined increment of the relative rotor-stator position between two timesteps is not constant. Therefore, the results are analysed at a comparable rotor-stator position for each timestep. The exact value of the relative rotor-stator position is given for each result. Due to discrete timesteps, different diffuser vane numbers and different initial rotor-stator positions in the numerical model, the experimental measured rotor-stator positions could not be met with reasonable effort. The minimal bandwidth of the measurements by Ziegler [3] in position 2M' is $\frac{\Delta\varphi_M}{\varphi_{t,D}} = 0.0502$, whereas the maximum relative difference between the numerical and experimental rotor-stator position is $|\frac{\varphi_M - \varphi_N}{\varphi_{t,D}}| = 0.01381$. This relative difference is more than three times lower than the experimental bandwidth. The deviations of the rotor-stator positions between the numerical results with an identical blade pitch are due to rounding errors in the analysis because the zero point of the rotor-stator position had to be determined manually.

The flow topology in the rear part of the centrifugal impeller is characterised by the relative velocity magnitude in

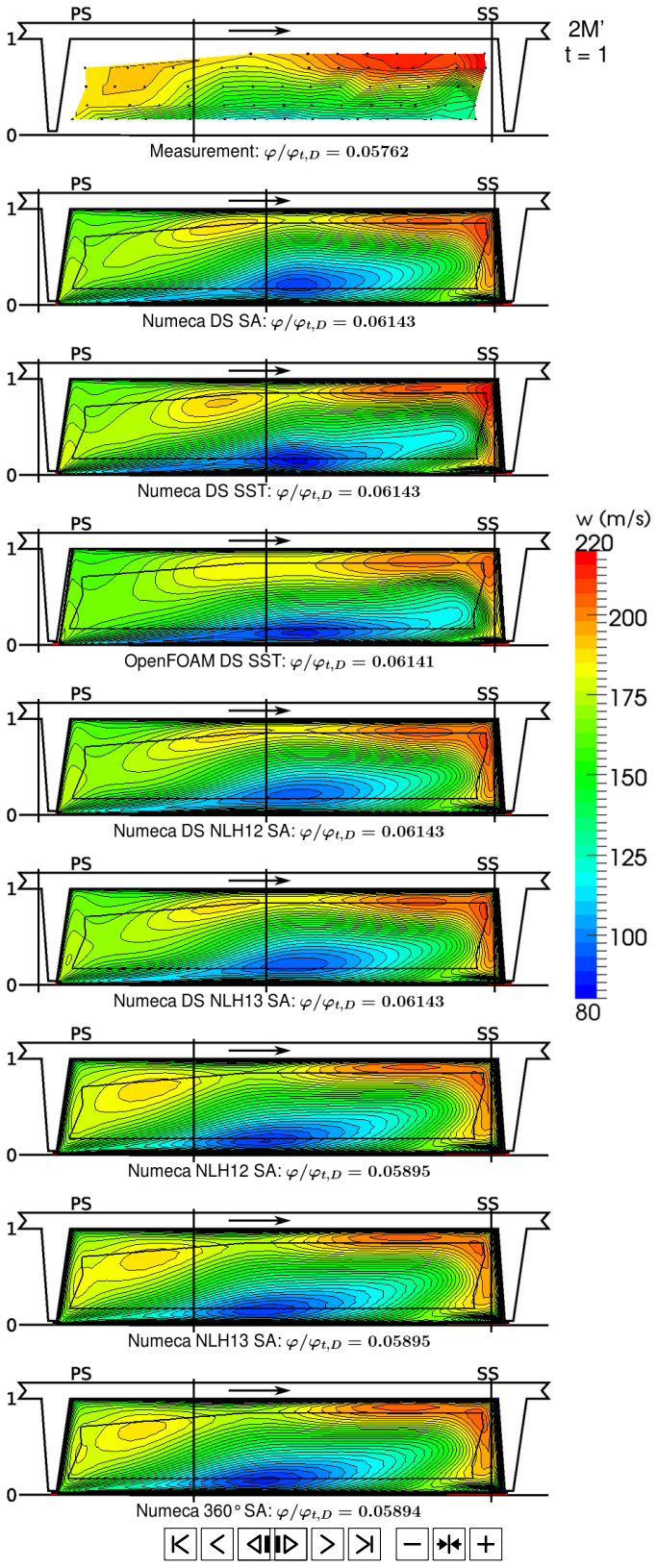

FIGURE 7. RELATIVE VELOCITY - POSITION 2M'

* In order to play these animations inside the electronic pdf version, you will need a reader with full JavaScript support, for example the Adobe Reader, which is available for most operating systems.

Fig. 7. Two main areas can be determined, the wake region with low momentum fluid near the casing and the suction side, and the jet region near the pressure side and the hub. Between those two regions the isotachs are compressed. The formation of the jet and wake region is sufficiently described in the literature. Both regions are influenced by the vaned diffuser in an unsteady manner. The area with lower relative velocity near the casing is thus not only a result of the coriolis force, which is acting on the fluid particles in the relative frame of reference and is related to the separation of fluid with high and low momentum fluid, but also as impounding reaction from the diffuser vane. The principle flow topology can be captured by all CFD results. The occurrence of the numerical results are slightly different when compared to the experimental results, especially the wake region is extended over a larger area of the channel. In all timesteps the numerical results with Spalart-Allmaras turbulence model and scaled diffuser are almost identical. The same holds true for the results with Spalart-Allmaras turbulence model and real diffuser blade count. Whereas both results with k-ω SST turbulence model are similar, especially the area of low relative velocity near the suction side. The influence of the diffuser leading edge is captured in all numerical results. Thus, the relative position of the low relative velocity near the casing depends on the number of diffuser vanes. A comparison of results between both diffuser geometries can therefore only occur on the basis of the relative position of the diffuser leading edge. The relative velocity near the pressure side is underpredicted in all CFD results, whereas the simulations with real diffuser count show slightly better results. The tip gap is a crucial parameter if analysing the local flow topology in a centrifugal impeller as already observed by Weiß [15].

Measurement Position 4M

The unsteady results of the absolute velocity magnitude are plotted in Fig. 8. For file size reasons, only every second timestep was inserted into the animations. In order to be able to compare both simulated diffuser geometries, the aspect ratio of the results with scaled diffuser was adjusted. The minimum bandwidth of the measured rotor-stator position is $\frac{\Delta\varphi_M}{\varphi_{t,D}} = 0.0293$ whereas the maximum difference between numerical and experimental rotor-stator position is $|\frac{\varphi_M - \varphi_N}{\varphi_{t,D}}| = 0.00660$. For position 4M it is more difficult to give a global assessment of the numerical results as there are no clear tendencies. In this position the accordance between numerical and experimental results depends on the considered timestep. There is a good agreement in some timesteps like t=1. The area of higher absolute velocity near the casing and lower absolute velocity in the area near hub and pressure side is predicted by all computations.

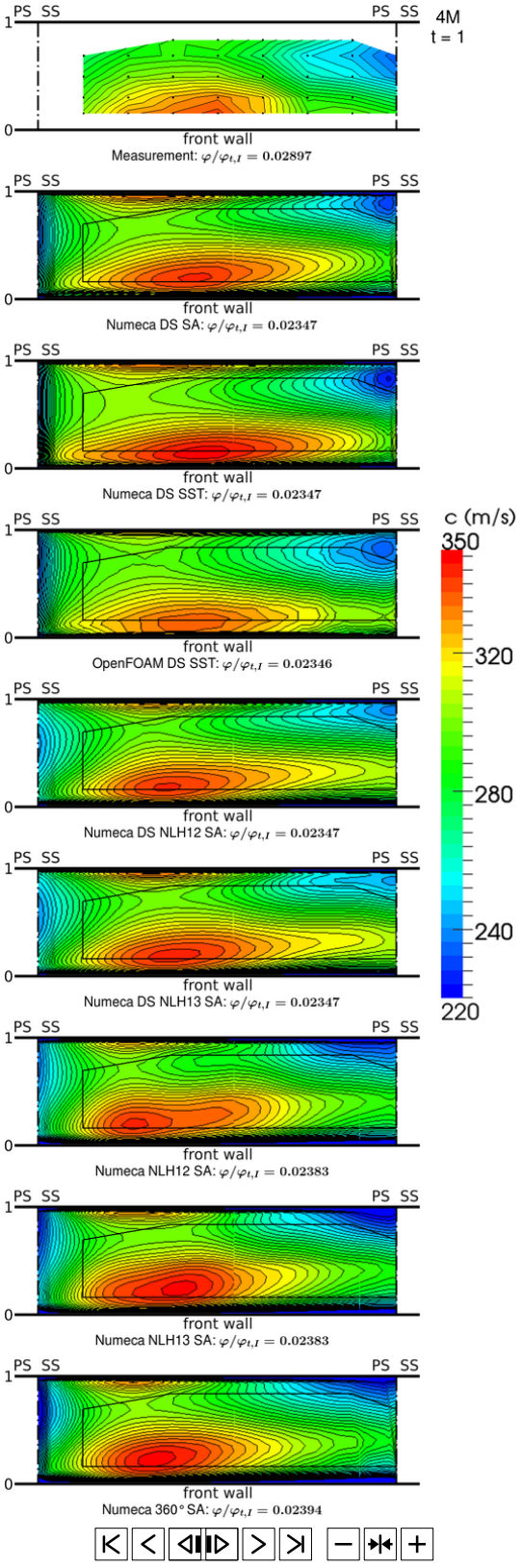

FIGURE 8. ABSOLUTE VELOCITY - POSITION 4M

However, the opposite is apparent in timestep t=5**. The results of the computations in the time domain show local areas with higher absolute velocity. These are only indicated in the experimental results. The vertical area in the mid channel can be assigned to the wake of the impeller blade. Unfortunately, no L2F measurements were possible in this region. Because there are no seeding particles available. Thus, this axial row of L2F probe points directly downstream of the impeller trailing edge is not available in the analysis of the experimental data. Hence, the experimental isotachs are based on the remaining probe points. It should therefore be taken into account that the wake area of the impeller blade is certainly present as numerically predicted by the computations in the time domain. In contrast, the NLH calculations in the frequency domain do not show such a strong wake. Moreover, the distribution of the absolute velocity downstream of the rotor-stator interface is much smoother. Both results with three harmonics show a slightly higher value of the wake in timestep t=5** than the results with two harmonics. Thus, with an increasing number of harmonics more unsteady effects can be captured. However, the resolution is still far behind the results of the simulations in the time domain.

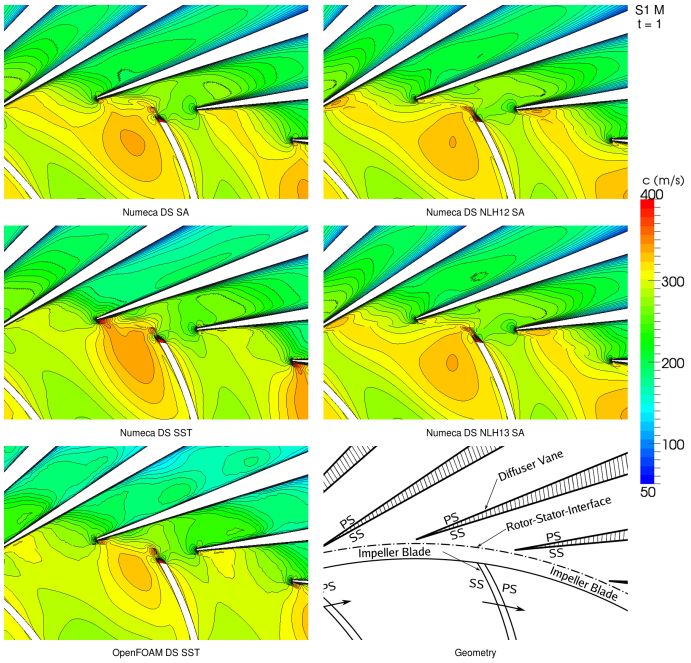

FIGURE 9. ABSOLUTE VELOCITY - ROTOR-STATOR INTERFACE

S_1 Surface Rotor-Stator Interface

In order to gain a better understanding of the flow topology in the area between impeller and diffuser, the flow is visualised at a geometric S_1 surface as defined by Wu [16] at 50% span height. Only the first timestep can be shown, because of file size reasons. The analysis is done based on the relative differences between the numerical results with domain-scaling approach, because there were not yet any experimental results published for this S_1 surface. As already described, the computational domain was restricted to one impeller and two diffuser passages. For a better visualisation, the numerical results are duplicated in circumferential direction. Therefore, the flow topologies in each impeller and every second diffuser passage are identical.

The first timestep of the absolute velocity magnitude is plotted in Fig. 9. In all results the wake region in the rear part of the impeller, visualised by the higher absolute velocity, is clearly distinct. Despite the same relative rotor-stator position, the respective occurrence of the wake-region is different in all calculations. The influence of the rotor-stator interface is almost negligible in the results of the time domain except for very small inaccuracies due to the interpolation. In contrast, the results of the computations in the frequency domain show a relatively strong discontinuity between both sides of the rotor-stator interface. This can be clearly seen due to a jump of the isotachs between both blade rows at the interface. The calculation with three harmonics shows in that case no clear advantage compared to the two harmonics. Furthermore, there is a strong compression of the impounding area upstream of the diffuser leading edge due to the rotor-stator interface in the results of the NLH simulations. As the Numeca computations were done with the same mesh, the discontinuities at the rotor-stator-interface can be attributed to the numerical model. The results with k-ω SST turbulence model with Numeca and OpenFOAM show a good agreement. There is also a small inaccuracy at the rotor-stator interface due to the interpolation between both blade rows.

S_1 Surface Diffuser

The absolute velocity magnitude at 50% span height of the diffuser is considered in Fig. 10. As already mentioned, the flow topology is identical in every second diffuser passage. From a high level between impeller and diffuser the absolute velocity is decelerated in the wedge type diffuser. Thus, the pressure rises in the vaned diffuser. As already expected by Ziegler based on the measurements in position 7M, there is a higher loading of the suction side of the diffuser vane in this operating point and with this radial gap. The absolute velocity at the suction side is very small in all numerical results, which indicates a separated flow. A similar behaviour was observed by Boncinelli et al. [4]. The

**only available in the pdf version

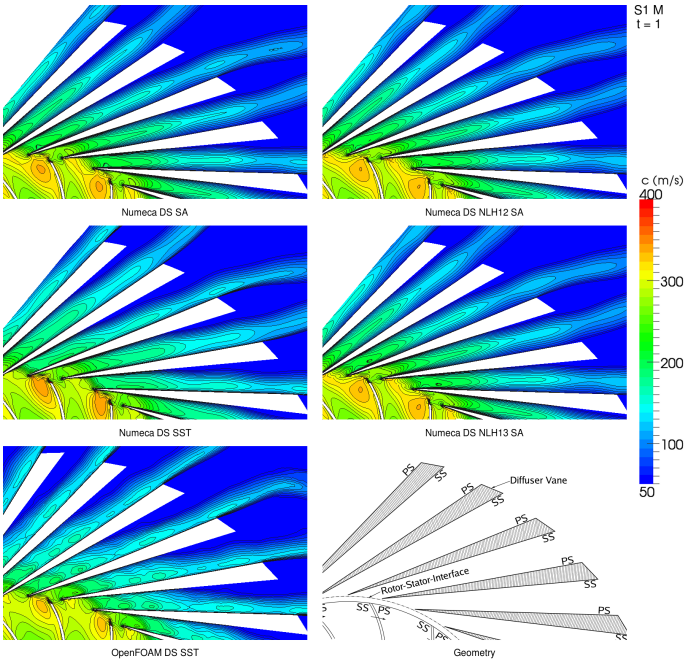

FIGURE 10. ABSOLUTE VELOCITY - VANED DIFFUSER

steady state results of him showed a separation at the pressure side in operating point P1. This separation was completely eliminated in the corresponding unsteady results and thus the loading of the suction side was increased. The separation point on the plain suction side of the results with k-ω SST turbulence model is located further upstream compared to the results with Spalart-Allmaras model as shown in Fig. 10. It can be assumed that the determination of the exact position of this separation point will not be possible with both turbulence models. However, the results with k-ω SST model have the best agreement with the measurements in position 7M as shown in Fig. 6. Therefore, the separation point further upstream is more probable and thus the results with k-ω SST model are more reliable.

Due to the periodic boundary condition two diffuser passages were simulated. Even if it is not visualised in Fig. 10, for the sake of completeness, it should be mentioned, that there is a backflow in all Numeca results from one diffuser trailing edge to the outlet boundary. Due to the displacement effect of this backflow, the jet streams of the two diffuser passages are merging in the vaneless area downstream of the diffuser vanes. The beginning can already be seen in Fig. 10. There were very small Mach numbers measured in position 8M (cf. Fig. 2) in the wake of the diffuser vanes. In the real geometry there is a large collector downstream of position 8M with a large area expansion. Thus, there will be no backflow from this collector to the vaneless area downstream of the wedge-type diffuser. Hence, the flow topology of the Numeca results downstream of the diffuser vane has to be considered as wrong. For the sake of completeness, in the Numeca computations the *Backflow Control* option did not work with *Expert Parameter BCKFLO=0* and was not tested with *BCKFLO=1*. It is likely that the last option could fix the backflow, because the description in the Numeca user guide sounds similar to the newly implemented boundary condition in OpenFOAM.

Computational Time

It is hard to compare the computational effort between the two solvers Numeca and OpenFOAM objectively, as there are several influence parameters. First of all, the simulations were started with different initial solutions. Additionally, if using a block-structured hexahedral mesh, the unstructured solver could not benefit from local refinements in unstructured polyhedral meshes. Furthermore, in a parallel computation the number of cores is limited by the number of blocks in Numeca. Even this number is only theoretical, as the load balance will then be bad due to the different number of cells in each block. It is possible to split large blocks manually but this is very time consuming compared to the decomposition of an unstructured mesh. There was no speed up of the full annulus 360° computation with Numeca when increased the number of cores from 12 to 24. Contrary to that, OpenFOAM has shown a linear scalability up to 1000 cores, if at least approximately 50 k cells remain at one core. Moreover, additional acceleration techniques are available in Numeca compared to OpenFOAM. For an objective comparison of both implementations these shouldn't be activated. In consideration of these parameters no absolute values of computational time are given.

If the computational effort of different numerical discretisation schemes at the same mesh with an identical number of cores and acceleration techniques is considered within Numeca, the following is observed. The steady state computations have the lowest computational effort, followed by the NLH method. The effort of the unsteady domain-scaling method is higher than the NLH method.

CONCLUSION

Steady and unsteady computations of a centrifugal compressor stage with wedge-type diffuser were conducted. A density-based approach with full polyhedral mesh support was implemented in OpenFOAM in order to simulate a transonic turbomachine within OpenFOAM for the first time. The influence of different numerical discretisation schemes and turbulence models were analysed and compared to experimental results. The steady state simulations with mixing-plane show a very good agreement to the ex-

perimental compressor map. In contrast to that, the flow resolution in the vaned diffuser is very poor as shown in position 7M downstream of the vaned diffuser. All time averaged unsteady results have a larger total pressure ratio compared to the experimental result. This is mainly attributed due to the fact, that the value of the static pressure at the outlet has to be larger in order to achieve the same normalised massflow as the measurements. The larger static pressure in the simulations seems to be a result of the underprediction of losses, mainly in the vaned diffuser. Thus, the total pressure level at position 7M is larger in the time averaged results. But on the other hand the distribution is captured more precisely with the unsteady simulations, which is believed to be more important than the deviation of the total pressure ratio. The unsteady results of OpenFOAM and Numeca with k-ω SST turbulence model and scaled diffuser are very similar in position 2M' and 4M. The simulations with k-ω SST model show a better agreement with the experimental result than the computations with Spalart-Allmaras model. The NLH method has some shortcomings in the vicinity of the rotor-stator interface. However, the computational effort is smaller compared to unsteady simulations. The used turbulence model has a larger influence in position 2M' and 7M rather than the unsteady numerical approach.

REFERENCES

[1] Borm, O., 2012. "Instationäre numerische Untersuchung der aerodynamischen Rotor-Stator-Interaktion in einem Radialverdichter". Dissertation, Technische Universität München.

[2] Eckardt, D., 1976. "Detailed Flow Investigations Within a High-Speed Centrifugal Compressor Impeller". *Journal of Fluids Engineering*, pp. 390–402.

[3] Ziegler, K. U. M., 2003. "Experimentelle Untersuchung der Laufrad-Diffusor-Interaktion in einem Radialverdichter variabler Geometrie". Dissertation, Rheinisch-Westfälische Technische Hochschule Aachen.

[4] Boncinelli, P., Ermini, M., Bartolacci, S., and Arnone, A., 2007. "On Effects of Impeller Interaction in the 'RADIVER' Centrifugal Compressor". In Proceedings of ASME Turbo Expo, Montreal. GT2007-27384.

[5] Smirnov, P. E., Hansen, T., and Menter, F. R., 2007. "Numerical Simulation Of Turbulent Flows In Centrifugal Compressor Stages With Different Radial Gaps". In Proceedings of ASME Turbo Expo, Montreal. GT2007-27376.

[6] Borm, O., Balassa, B., and Kau, H.-P., 2011. "Comparison of Different Numerical Approaches at the Centrifugal Compressor RADIVER". In 20th ISABE Conference, Gothenburg, Sweden, 12th - 16th September 2011. ISABE-2011-1242.

[7] Borm, O., Jemcov, A., and Kau, H.-P., 2011. "Density Based Navier Stokes Solver for Transonic Flows". In 6th OpenFOAM Workshop, PennState University, USA.

[8] Hirt, C. W., Amsden, A. A., and Cook, J. L., 1974. "An Arbitrary Lagrangian-Eulerian Computing Method for All Flow Speeds". *Journal of Computational Physics*, pp. 224–253.

[9] gmsh, 2.5. `http://www.geuz.org/gmsh`.

[10] enGrid, 1.2. `http://sourceforge.net/projects/engrid`.

[11] Hoffmann, A., Grates, D., and Niehuis, R., 2005. "Numerische Untersuchung zur Laufrad-Leitrad Interaktion in einem Radialverdichter mit Keilschaufeldiffusor". In DGLR Jahrestagung. DLR-2005-161.

[12] Denton, J. D., 2010. "Some Limitations Of Turbomachinery CFD". In Proceedings of ASME Turbo Expo, Glasgow. GT2010-22540.

[13] Grates, D. R., 2010. "Numerische Simulation der instationären Strömung in einem Radialverdichter mit Pipe-Diffusor". Dissertation, Rheinisch-Westfälische Technische Hochschule Aachen.

[14] Bramesfeld, W., 1995. "Optimierung eines Laser-Zwei-Fokus-Meßsystems zur berührungslosen Geschwindigkeitsmessung in Turbomaschinen". Dissertation, Rheinisch-Westfälische Technische Hochschule Aachen.

[15] Weiß, C., 2002. "Numerische Simulation der reibungsbehafteten Strömung in Laufrädern von Radialverdichtern". Dissertation, Rheinisch-Westfälische Technische Hochschule Aachen.

[16] Wu, C.-H., 1952. A general theory of three-dimensional flow in subsonic and supersonic turbomachines of axial-, radial-, and mixed-flow types. Tech. Rep. TN-2604, NACA.